Asia-Pacific Journal of Science and Technology: Volume: 29. Issue: 01. Article ID.: APST-29-01-07. Research Article

APST

Asia-Pacific Journal of Science and Technology

https://www.tci-thaijo.org/index.php/APST/index

Published by the Research and Graduate Studies,
Khon Kaen University, Thailand

Adsorption studies on chitosan/bagasse nanocomposite surface for the elimination of hazardous Cr (VI) from wastewater

Rekha Goswami[1,2] and Abhilasha Mishra[3,*]

[1]Department of Environmental Science, Graphic Era (Deemed to be University), Dehradun, India
[2]Department of Environmental Science, Graphic Era Hill University, Dehradun, India
[3]Department of Chemistry, Graphic Era (Deemed to be University), Dehradun, India
[*]Corresponding author: abhi1680@geu.ac.in

Received 9 November 2022
Revised 15 December2022
Accepted 22 December 2022

Abstract

Heavy metal contamination drastically effects the ecosystem and human life. This work focusing on elimination of Chromium (Cr (VI)) ion from the synthetic wastewater using biodegradable and easy to use chitosan blended sugarcane bagasse nanocomposite. The nanocomposite was prepared via crosslinking of chitosan and cellulose nanocrystals with N, N-methylenebisacrylamide (MBA). The successful blending and crosslinking have been confirmed by using Fourier Transform Infrared Spectroscopy (FTIR), Field Emission Scanning Electron Microscopy (FESEM), X-Ray diffraction (XRD), Particle size analysis (PSA). The adsorption potential of the nanocomposite of heavy metal ion under different time duration, pH, dosage and initial chromium solution concentration were analysed using UV spectroscopy. The ideal pH was 4, equilibrium interface time was 90 min, adsorbent dose was 0.1 g, and beginning metal ion concentration was 100 ppm for the adsorption investigation. Ionic effect was also observed. The adsorption potential was evaluated using linear and nonlinear isotherm and kinetic models and results portrayed that the Langmuir Isotherm were best fitted in case of linear and Freundlich in case of nonlinear models, whereas follow Pseudo 2nd order reaction in case of linear and Pseudo 1st order reaction in case of nonlinear showing chemical bonding between the adsorbent (nanocomposite) and adsorbate (chromium ions). Thermodynamics parameters were analysed it confirms the spontaneous and favourable adsorption mechanism. Maximum desorption rate of 95% at 90 min contact time was observed in 0.1 M HCl, with five repetitive cycles.

Keywords: Adsorption, Chromium, Chitosan, Nanocomposite, Desorption

1. Introduction

The growth in industrial scale becomes hasty worldwide which results in the ingression of various unwanted heavy metal to the aquatic water system. Many industrial wastewater effluents contain metals such as Pb, Zn, Ni, Cr, Cu, and Hg, which are very hazardous and carcinogenic even at low concentrations. Due to non-biodegradable behaviour of heavy metals, it becomes substantially hazardous and cause environmental as well as human health damage [1-4] It causes problem and show toxic behaviour, even at modest level [5]. This study mainly deals with the removal of Chromium (Cr (VI)) metal ions from laboratory prepared aqueous solution. Trivalent and hexavalent chromium have differing chemical, biological, and environmental properties. It is also known to be as trace metal required at a very small quantity for the growth of several microorganism, on the other hand it the also show extreme toxicity level, known to be carcinogenic in behaviour also [6].

The majority of chromium wastewater is discharged from sources such as tanneries, textile, electroplating, steel production, and mining sectors, among others [7-9]. Due to their non-biodegradable nature, high toxicity, and ease of entry into the food chain, chromium heavy metals pose a concern to both humans and ecosystems [10]. It also causes cancer, renal and liver dysfunction, vomiting, ulcers, and skin discoloration, among others [11,12]. The concerned govern authorities WHO set limitations for chromium-ion-containing wastewater

discharge to surface waterbodies. Safe disposal levels up to 0.1 mg/L and 0.05 mg/L in surface waterbodies and drinking water respectively. In order to comply with this permissible limit, it is utmost important that all the concerned industries properly treat chromium wastewater to meet out the acceptable standards, prior to discharge into the natural environment [13].

Numerous conventional techniques have been used to treat wastewater containing heavy metals in order to lessen the impact of heavy metal pollution on the freshwater ecosystem and human health, including membrane separation, biological methods, TiO_2 photocatalysis, sedimentation, electroplating, precipitation, photocatalytic reduction, ion exchange, precipitation, adsorption, Fenton-like oxidation, replacement-coprecipitation. Some of these methods are unsuitable for chromium species eradication due to their resistance. Most existing technologies are expensive, produce secondary pollutants, use a lot of energy, process slowly, have poor adsorbent regeneration, and only remove a small amount of pollutant [14,15]

Adsorption method is remarkably used to treat wastewater. This method is flexible, less energy needed for working condition, easy to use, economic and repeatedly use of adsorbent make it cost effective also. Moreover, because adsorption is occasionally reversible, adsorbents can be renewed through an appropriate desorption procedure [16]. Using cheap and effective adsorbent to remove Cr (VI) from aqueous solutions has been reported in recent years. Various agro-based adsorbents are used, such as sweet lime peel, waste tea leaves, apple peel, banana peel, pine bark, rice husk, mangrove charcoal etc [17,18-24]. The non-conventional adsorbent show number of advantages such as efficient removal of the pollutant, cheaper than conventional adsorbents with very low transportation cost comparatively if available locally, simplest process is used for the lignin removal for the extraction of major portion from the raw material and require less maintenance cost. Therefore, cost-effective adsorbent is one of the factors that keeps on mind while fabricating adsorbents. In this study nanocomposite formulation was done by using chitosan as matrix and cellulose nanocrystals (CNCs) act as nanofillers, for reinforcement the nanocomposite was crosslinked with N, N-methylenebisacrylamide (MBA).

Nontoxic, biodegradable, and soluble in basic media, chitosan forms high-viscosity solutions. Chitosan films and chelates. De-acetylating chitin produces β-(1→4)-linked D-glucosamine, one of the most prevalent natural polymers. Due to its chemical, biological, and physical qualities, chitosan has several uses. Food, agriculture, cosmetics, biomedicine, pharmaceuticals, fibers, drinking water, wastewater treatment, toiletries, textiles, and paper industry use it. [25]. Due to its amine functional groups, chitosan selectively adsorbs metal ions [26-28]. Chitosan's stability in acidic conditions and selective adsorption of heavy metals are improved via chemical treatment. Chitosan can be modified by crosslinking [29,30], grafting [31], carboxy-methylation [32], and blending [33,34]. Unmodified biomass had poorer absorption capability. Thus, one of the most effective ways to boost biomass's water pollution absorption is chemical alteration.

A natural biopolymer called cellulose is produced from the biomass of plants, including trees, vines, and straws. This is one of the explanations for the widespread availability and use of cellulose. The production of cellulose from the sources can be accomplished using biological, chemical, and mechanical procedures. The term "nanocellulose" refers to cellulose that was produced at the nanoscale (NC) [35]. NC is a successful adsorbent for the elimination of contaminants from wastewater due to its high specific nano-dimension area, many hydroxyl groups, and exceptional mechanical characteristics. NC has been used extensively as an adsorbent, especially for the removal of dangerous colors and heavy metals from water [36-38]. The use of NC in the process of removing chromium ions from an environment is constrained, nevertheless, due to its low adsorption capability. By modifying the NC's surface to boost its affinity and capacity for adsorbing the desired ions, this restriction can be overcome. Studies have been conducted using cellulose- and chitosan-based polymers for the adsorptive removal of heavy metals and dyes. In this study, a novel biocomposite adsorbent was made from the two most abundant natural resources (nanocellulose and chitosan) that was developed by extracting nanocellulose from sugarcane bagasse, to remove chromium ions from synthetic wastewater. In order to increase the stability of chitosan molecules and nanocellulose during adsorption study it was crosslinked thermally with methylene-bis-acrylamide (MBA) by casting process at a constant temperature. Several limiting parameters were investigated during the adsorption process, including pH value, contact duration, initial metal concentration and adequate dosage. In addition, the isotherms, kinetics (linear and nonlinear) and thermodynamics studies were performed to observe the adsorption behavior. In previous research, several kinds of catalysts and initiators were utilized to accelerate the adsorption reaction (with MBA serving as the crosslinker), and this was done solely for the purpose of the development of hydrogels and super hydrogels [39,40,41]. In this study we use novel and simple one-way process for the creation of a nanocomposite adsorbent utilizing MBA alone, to the best of our knowledge, this has not been reported without the use of any extra chemicals to either start or speed up the reaction. This research employs a novel strategy that has never been used in any prior investigation of nanocellulose.

2. Materials and methods

2.1 Reagents used

The raw sugarcane bagasse was obtained from CIPRII Saharanpur plant in dried form. All the chemicals such as Chitosan (90% deacetylated), Sodium hypochlorite (13%), H_2SO4 (97%), MBA (99%), Glacial acetic acid (99%), Potassium dichromate ($K_2Cr_2O_7$), Diphenyl carbazide (DPC) as indicator were purchased from Sigma Aldrich and used in its original form during experimental work. No distillation or purification procedures were utilised, and all the compounds were of analytical quality.

2.2 CNCs extraction process

The received sugarcane bagasse (SGB) firstly washed properly and dried for 5-10 days at room temperature. After adequate washing it was treated preliminary and chemically in order to enhance its metal uptake efficiency. For primary alkali treatment, known amount of SGB treated with NaOH (0.1 M) and stirred at 300 rpm for 10 h. After attaining neutral pH, the sample was further treated with 13 % NaOCl solution for bleaching purpose, stirred at 450 rpm for 8 h and finally treated with 2 % acid solution, stirred for 60 min at 50°C for to extract out CNCs. After completion of hydrolysis process, 10 folds cold deionized (DI) water were added number of times to get pH 7. Now, the extracted CNCs suspension were centrifuged at rotation per min of 6500 for 30 min, then after centrifuged CNCs pulp washed again and completely dried at 80°C to obtain fine powder of CNCs and stored for further research study.

2.3 Synthesis of nanocomposite membrane-based adsorbent

A suspension of the CNCs was made by dispersing around 2.0 g of cellulose nanocrystals in 50 mL of DI water, followed by the addition of 0.5 g of chitosan that had been dissolved in 30 mL of 2% acetic acid. Afterward, 0.04 g crosslinking agent (MBA) was added and stirred for 60 min. After that, the mixture was put into a Petri dish and heated at 70°C for 8 h. After complete drying, the resulted sample cools down at room temperature and further distilled water added to make the membrane detach from the surface. After frequent washing in order to remove all the unreacted particles, it finally dried well with bloating paper and preserved for further analysis. The resulted membrane was labelled as chitin nanocrystals (ChNC)+MBA.

2.4 Characterization of synthesized nanocomposite

2.4.1 Particle size analysis

The measurements were taken with a Malvern 3000 Zetasizer NanoZS (Malvern Instruments, Malvern, WR14 1XZ. UK). Using dynamic light scattering, this instrument calculates particle sizes and distributions from data gathered on particles moving with Brownian motion.

2.4.2 FTIR spectrum analysis

The functional group entities were analysed using FTIR, Model-L160000V, Make- Perkin Elmer, Waltham, MA, USA. During analysis the spectra was analysed in the frequency ranges from 4000 to 1000 cm-1 at normal room temperature.

2.4.3 XRD spectral analysis

To evaluate the crystallinity of the ChNC+MBA nanocomposite before and after metal ions adsorption and after desorption XRD Rigaku Ultima IV (Japan) used. Cu target Kα radiations (1.154 nm) were scanned at 2 nm/min between angles 4 and 90. Scherrer equation determined average crystallite size (nm).

$$D = \frac{K\lambda}{\beta \cos\theta} \tag{1}$$

where, K = correction factor (0.91), λ= 0.154 nm, θ= diffraction angle, β = FWHM (radians), D = crystallite size (nm).

For crystalline index (CI) following equation is used:

$$CI\ (\%) = Ac/(Ac + Aa)\ x\ 100 \tag{2}$$

A_c = crystalline peaks total area and A_a = amorphous region total area.

2.4.4 Field Emission Scanning Electron Microscopy (FESEM) micrographs analysis

To detect the structural changes after fabrication with other polymers the resulted membrane-based adsorbent were analysed using FESEM. To analyse the structural structure of the samples, operating voltage of 10 to 25 KV was used. The samples were thinly coated with gold layer before examination using a sputtering process for improved results.

2.4.5 Ionic strength

After adding NaCl to increase the ionic strength to 0.2-1.0 mol/L, 0.1 g adsorbents and 50 mL metal ion solution (100 mg/L) were shaken for 24 h at 30°C.

2.5 Adsorption study

To investigate the ChNC+MBA, potential towards Cr (VI) ions removal, batch study was conducted at room temperature 30°C. For Batch study, 100 mL metal ion solution and the necessary adsorbents were taken in 250 mL stopper conical flask. These tests were done at the appropriate pH value, contact duration, adequate dose of adsorbent, and beginning metal ion concentration. A variety of Cr (VI) solutions with varying beginning concentrations were generated by appropriately diluting a stock solution containing 1000 ppm of Cr (VI).

To optimize pH, we utilized 50 mL of a metal ion solution with 100 mg/L. NaOH or HCl (0.1 M) was used to adjust pH. After adding metal ion solutions to 0.1 g of nanocomposite, the mixture was agitated for 2 h at 30°C. Cr (VI) concentration of 100 mg/L and a pH of 4 were used to study the effect of adsorbent dose on percent removal. A solution of Cr (VI) with concentrations from 20 mg/L to 100 mg/L, a pH of 4, a contact length of 2 hours, and an adsorbent dose level of 0.1 g/L was used to study the influence of beginning concentration. The same procedure was used to study contact time.

Following American Public Health Association (APHA) and American Water Works Association (AWWA) standards for water and wastewater inspection, the flask's contents were filtered through filter paper and tested for the amount of Cr (VI) that was left using a HACH-DR-4000 UV visible spectrophotometer with 1,5-diphenylcarbazide in acid medium. All tests were repeated to assure uniformity. After a thorough batch study, the removal rate and adsorbed metal ion were calculated using the Equation 3 and 4.

$$\text{Removal Rate}(\%) = \frac{\text{Metal Conc}_{(\text{Initial})} - \text{Metal Conc}_{(\text{Final})}}{\text{Metal Conc}_{(\text{Initial})}} \text{x}100 \quad (3)$$

$$\text{Adsorbed metal ion}(\text{mg/g}) = \frac{C_0 - C_e \text{ x } V}{m} \quad (4)$$

whereas C_0 denotes initial concentration of Cr (VI), C_e denotes final Cr (VI) concentration after adsorption, V is total volume of the working solution taken in litre and m denotes adsorbent dried weight in gm.

During adsorption, metal ion ranging from 20 to 100 mg/L were measured. The potentiality of a 50 mL working solution containing 0.1 g adsorbent was examined using linear and non-linear isotherm models. For 24 h, the mixture was stirred at 30°C.

Linear and non-linear models were used to analyse adsorption kinetics by contacting 100 mL of a metal ions solution with an initial concentration of 100 mg/L with 0.2 grams of adsorbents at 30 degrees Celsius and pH 4.0. The Linearized isotherms represented as Equation 5 and 6:

$$\frac{C_e}{q_e} = \frac{1}{q_m} C_e + \frac{K_L}{q_m} \quad (5)$$

$$\ln q_e = \ln K_F + \frac{1}{n} \ln C_e \quad (6)$$

C_e (mgL^{-1}) stands for metal ions concentration (at equilibrium), q_e (mgg^{-1}) for the amount of metal ions adsorbed (at equilibrium), q_m (mgg^{-1}) for maximum adsorption capacity, K_L and K_F (Lmg^{-1}) for Langmuir and Freundlich constants, and 1/n for adsorption intensity in the corresponding equations. The Non-linear isotherms represented as Equation 7 and 8:

$$q_e = \frac{q_{max} K_L C_e}{1 + K_L C_e} \quad (7)$$

$$q_{e} = K_f \text{ x } Ce^{(1/n)} \quad (8)$$

The equation indicates the nanocomposite's adsorption capacity (q_e), maximum adsorption capacity (q_{max}), Langmuir adsorption constant (K_L), and metal ion concentration (C_e) (equilibrium). K_F (mg g^{-1}) is the Freundlich constant for adsorption tendency, and 1/n is for surface heterogeneity.

To know about the occurrence of interaction during adsorption process kinetics models were used. The linear as well as nonlinear form of Pseudo first order (PFO) and Pseudo second order (PSO) were analysed and represented below in Equation 9 ,10, 11 and 12:

$$\ln(q_e - q_t) = \ln q_e - k1\, t \tag{9}$$

$$\frac{t}{qt} = \frac{1}{k2qe2} + \frac{t}{qe} \tag{10}$$

$$q_{t} = q_e(1-e^{-k1t}) \tag{11}$$

$$q_{t} = \frac{q_{e^2}\, k_2\, t}{1+q_e\, k_2\, t} \tag{12}$$

qe (mgg^{-1}) and qt (mgg^{-1}) represent adsorption capacity (at equilibrium) and duration t (min), respectively, whereas K_1 and K_2 (g mg/min) represent PFO and PSO rate constants.

The impact of the solution temperature was evaluated by adding 0.1 g of nanocomposite to a series of flasks that each contained 50 mL (100 mg/L) of a metal ions solution with a pH of 4.0. The flasks were arranged in a sequence. Temperatures in the range of 25 to 40 degrees Celsius were recorded.

Following equation estimated the thermodynamic equilibrium constant (K_d, L/g) for metal ion adsorption on nanocomposite adsorbents at 293, 298, 303, and 308 K.

$$Kd = \frac{Qe}{Ce} \tag{13}$$

The following equations determined Gibbs free energy change (ΔG◦), enthalpy change (ΔH◦), and entropy change (ΔS◦):

$$\text{In Kd} = \frac{\Delta S^\circ}{R} - \frac{\Delta H^\circ}{RT} \tag{14}$$

$$\Delta G^\circ = -RT\ \text{In Kd} \tag{15}$$

where R stands for the universal gas constant (equal to 8.314 J/(moL K)) and T stands for the absolute temperature (K). Values of ΔH° and ΔS° can be determined from the slope and intercept of the line connecting ln Kd to 1/T.

qe (mg/g^1) and qt (mg/g^1) represent the adsorption capacity (at equilibrium) and time t (min), respectively; qt (mg/g) displays the adsorption capacity at time t; K_1 (g/mg/min) and K_2 (g/mg/min) stand for the rate constants of PFO and PSO, respectively.

2.6 Regeneration/desorption study

After successful adsorption of Cr (VI) ion onto nanocomposite, it is desorbed to avoid fouling problem. In order to do that, 0.1 M HCl and 0.1 M NaOH were used, about 50 mL of each acid as regenerating agent were taken and metal loaded adsorbent was added. The desorption tendency of each reagent was observed under the time duration of 30-120 min. By using following equation 16 desorption ratio was estimated. Total five cycles were run to observe the effectiveness of the nanocomposite.

$$\text{Desorption Ratio} = \frac{\text{Desorbed metal ion concentration}}{\text{Adsorbed metal ion concentration}} \text{ x } 100 \tag{16}$$

3. Results and discussion

3.1 Instrumental analysis

3.1.1 Nanocellulose particle size

The built-in Zetasizer application was used to automatically analyse and compute light-scattering data, which was then used to generate hydrodynamic diameter dimensions. The DLS-obtained particle size distribution is shown in Figure 1; it reveals that 95.5% of particles are under nano-dimension ranging from 100-300 nm.

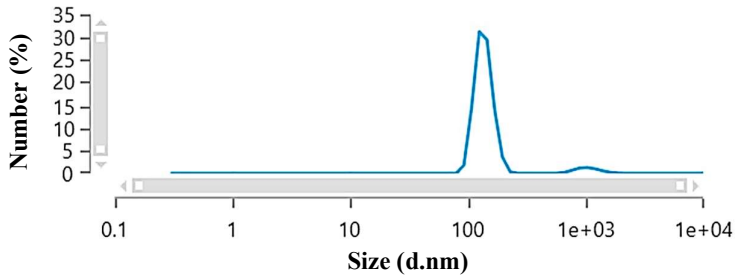

Figure 1 Particle size distribution of nanocellulose.

3.1.2 Fourier transform infrared spectroscopy (FTIR) spectral analysis

In Figure 2, we observed the infrared spectra of chitosan, MBA, CNCs and nanocomposite. Chitosan Spectral bands shows prominence at 3632 cm^{-1} for O-H stretching signals, band at 3035 cm^{-1} denotes the availability of OH functional group arises due to intermolecular hydrogen bonding. The absorption frequency at around 2945 cm^{-1} can be attributed to C-H symmetric stretching, 1560 cm^{-1} peaks attributed to the NH_2 group peak, the symmetrical deformation of CH_3 and CH_2 group confirmed at 1362 cm^{-1}. The peak at 1151 cm^{-1}, confirmed the existence of (1-4)-glycosidic band in poly saccharide unit, 1065 cm^{-1} peak is due to CH-OH in chitosan. [42-46]. Pure MBA spectral data showed peak at 3301 cm^{-1} designated to N-H stretching vibration, observed peak at 3062 cm^{-1} has been assigned to C=CH stretching vibrations and 2954 cm^{-1} attributed to C-H stretching vibration , 1659 cm^{-1} is assigned to C=O stretching mode showing Amide I band, 1617 cm^{-1} is essentially due to C=Cα stretching mode, band at 1539 cm^{-1} is assigned to deformation of (N-H) moiety showing Amide II band, observed 1301 cm^{-1} is assigned to C-N stretching vibration showing Amide III band [47]. Acid hydrolysed CNCs showing bands at 3372 cm^{-1} revealing the presence of intramolecular hydrogen bonds for cellulose I due to O-H stretching group, 2879 cm^{-1} attributed to C-H stretching, due to adsorbed water molecules, O-H bending was confirmed at 1638 cm^{-1}, 1429 cm^{-1} is due to CH_2 scissoring motion in cellulose, strongly confirms cellulose I content, 1321 cm^{-1} and 1163 cm^{-1} peak assigned to CH_2 wagging and C-O-C asymmetric stretch vibration respectively was a proof of the presence of crystallized I cellulose, Spectral peak at 1050 cm^{-1} has been assigned to C-O-C pyranose ring stretching vibration [48,49]. Spectral band observation after nanocomposite composite formulation, showed band at 3321 cm^{-1} confirms the presence of OH and amine group (N-H), the observed broadness in the band structure confirms the participation of OH and NH functionalities in the hydrogen bond formation. The spectral band shifted towards lower wavenumber from 2945 cm^{-1} of Chitosan, 2954 cm^{-1} of MBA to 2904 cm^{-1} in the prepared nanocomposite confirms the strong interaction between the polymer showing CH stretching, which show strong bonding ,1634 cm^{-1} showing imine bond (C=N) formation confirms the successful crosslinking with MBA molecules, shifting of the OH and NH band confirm its participation in blending and crosslinking process [50]. The Amide group (NH_2) shifted towards lower wavenumber from to 1560 cm^{-1} of Chitosan, 1539 cm^{-1} of MBA to 1530 cm^{-1} in the prepared nanocomposite. Spectral band at 1372 cm^{-1} showing CH_2 wagging and twisting vibration, bands shifted from 1163 cm^{-1} in CNCs to 1154 cm^{-1} attributed to CO stretching vibration, shifted from 1050 cm^{-1} to 1033 cm^{-1} attributed stretching vibration of C-O-C in the prepared nanocomposite [51].

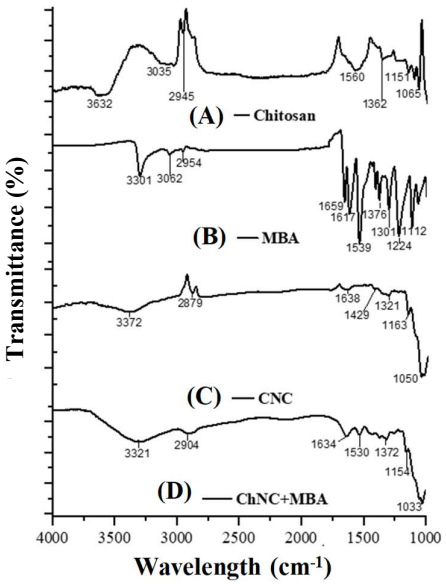

Figure 2 IR Spectra (A) Chitosan (B) MBA (C) CNCs (D) Nanocomposite.

3.1.3 X-ray diffraction (XRD) analysis

Figure 3 shows the XRD patterns of CNCs, nanocomposite before and after adsorption and after desorption. Acid hydrolysed nanocrystals revealed crystalline peak at angles 2θ=15.72°, 22.54°, and 34.55°, confirming cellulose I structure. 110, 200, and 004 crystallographic planes, which indicate cellulose I structure, may explain the peaks. Chitosan and MBA formed new peaks at 2θ = 11.67º, indicating its hydrated crystalline structure and 2θ =16.25°, 18.86°, 22.56° and 26.6° revealed strongly crystalline behavior of MBA, confirms the presence of MBA, results in successful crosslinking between all the components used during the formulation of the adsorbent nanocomposite [52]. It was noted that after metal ions adsorption, some peaks are disappeared and some peaks were shifted to 2θ = 16.13º, 22.28º, 26.38° and 34.39º, the observed decreased diffraction peaks after metal ion adsorption confirms the adherence of metal ions during the batch study. XRD analysis after desorption was also done to check its stability and the peaks were found at 2θ = 16.63º, 22.67º, 26.84º and 34.63º, increased intensities of the observed peaks showing the stability of the nanocomposite [53].

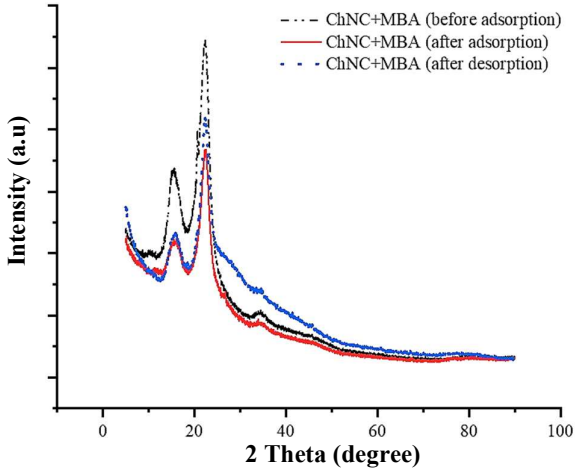

Figure 3 XRD Spectra CNC nanocomposite before and after adsorption nanocomposite after desorption.

The average crystallite size and crystallinity index (CI), determined using (Equation 1 and 2), were 1.1 nm, 1.3 nm, 1.6 nm, 1.2 and 72%, 14%, 11%, and 13% for acid hydrolysed CNC, nanocomposite before, after, and after desorption, respectively. Crystallinity Acid hydrolysed CNC had a higher crystallinity index than nanocomposite before, during, and after adsorption. Nanocrystalline plains may arise after chemical treatment

removes lignin or amorphous material from cellulose. Metal ions adhere to adsorbent surfaces when crystallite size increases from 1.1 to 1.6 mm and crystallinity index decreases from 14% to 11%. Whereas decrease in crystallinity size from 1.6 to 1.2 nm and increase in crystallinity index from 11% to 13% shows successful desorption activity of the nanocomposite [54].

3.1.4 FESEM

The porous structure of the nanocomposite is clearly visible in figure 4 which confirms its permeable behaviour for easy diffusion rate during adsorption process. Figure 4 also shows the nanocomposite after successful adsorption process. The porous structures are filled completely after adsorption confirms the interaction between heavy metals and nanocomposite materials [55].

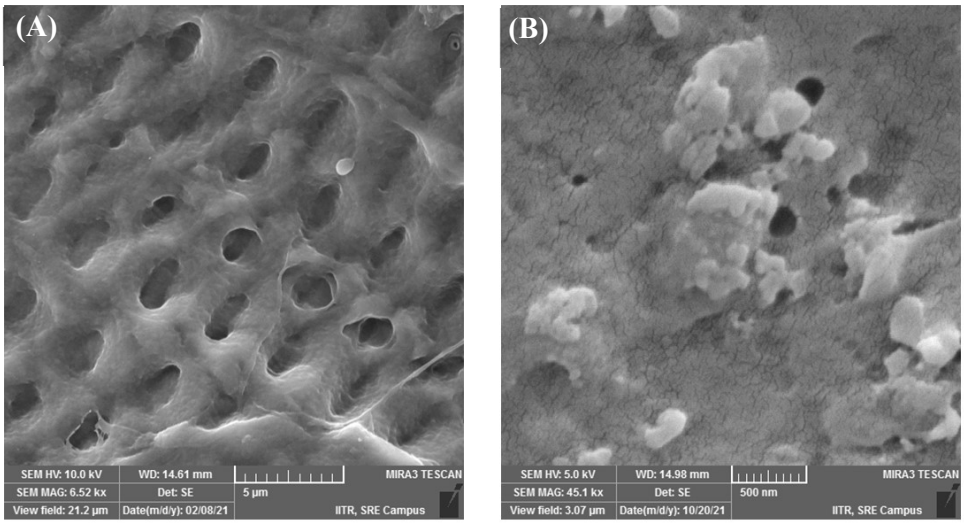

Figure 4 FESEM micrographs of ChNC+MBA nanocomposite (A) before and (B) after adsorption.

3.1.5 Ionic effect study on metal ion removal rate

Industrial wastewaters have high quantities of salts, reducing target pollutant removal efficiency. This requires frequent regeneration, increasing operation expense. Figure 5 shows the effects of ionic strength on nanocomposite metal ion adsorption using an ionic medium of 0.2-1.0 mol/L NaCl. NaCl did not affect nanocomposite Cr (VI) adsorption at 0.2 to 0.4 mol/L^1. However, Cr (VI) removal dropped from 76% at 0.2 mol/ L to 36% at 1.0 mol/L. These findings demonstrate that Cl^- and Na^+ ions in solution can marginally compete with Cr (VI) for nanocomposite sorption sites at low concentrations, whereas Cr (VI) and nanocomposite electrostatic interaction was inhibited at high NaCl concentrations [56,57].

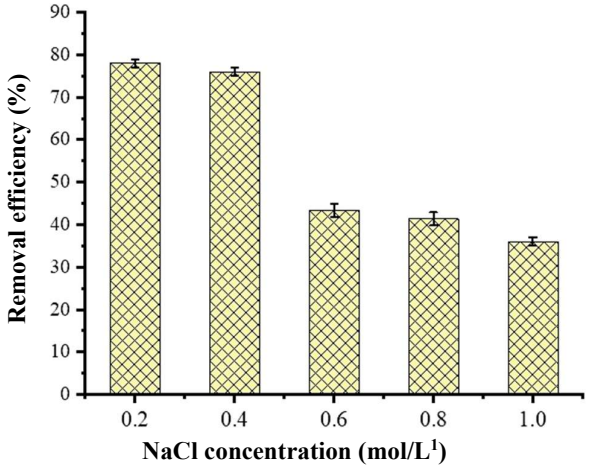

Figure 5 Ionic effect on the removal efficiency of the nanocomposite

3.2 Adsorption study analysis

Adsorption method is well renowned process for the removal of heavy metal from aqueous solution, due to its cost effectiveness it is highly recommended. In this study ChNC+MBA nanocomposite were analysed during batch study by altering various factors such as solution pH, dosage, contact duration, metal ion initial concentration to get optimized condition for maximum elimination of the heavy metal ions. The adsorption mechanism illustrated in Figure 6.

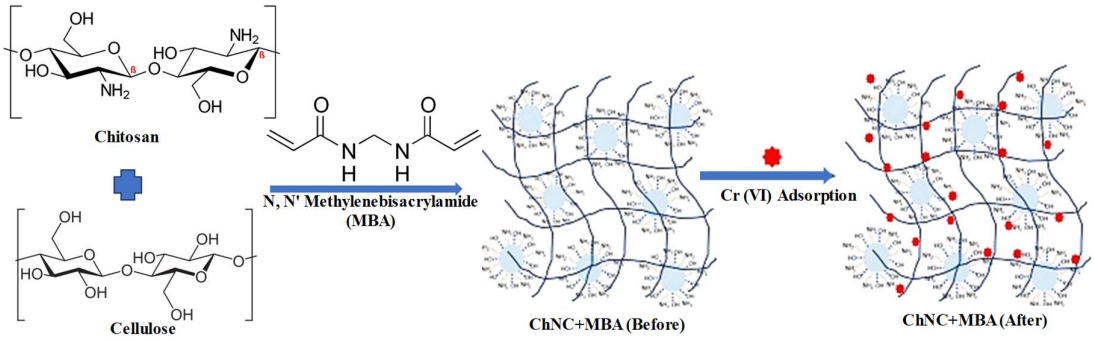

Figure 6 Schematic illustration of chromium ions removal mechanism.

3.2.1 pH and adsorbent dosage effect

pH plays significant role during adsorption process due to modification in surface chemistry as well as in ionization degree. Therefore, it seems to be one of the major parameters to be check during metal ion adsorption. For this study the pH ranges from 3 to 9 for the initial metal ion solution, at fixed adsorbent dosage of 0.1 g and time duration fixed to 90 min to analyse the optimum pH for maximum metal ion removal at normal room temperature. Observed variation in the results given in Figure 7A. It is clearly shown in the graph that on increasing pH from 3 to 4 the removal efficiency of the metal ion is maximum. The maximum elimination of metal ions was observed at pH 4. After it the removal rate decreases as the pH value increase, it was due to decrease in the proton concentration, results in lowering of proton competence with metal ions. Most chromium is in the Cr (VI) and Cr (III) oxidation states, and its stability relies on pH. The hydrolysis process of the dichromate ion ($Cr_2O_7^{2-}$) produces Cr (VI) at $HCrO^{4-}$. $HCrO^{4-}$ becomes $Cr_2O_7^{2-}$ and other forms when pH rises. The $HCrO^{4-}$ form of Cr (VI) was the dominating species at pH 4 and adsorbed preferentially on the adsorbents. The huge amount of H^+ ions at low pH values of 4 neutralize the negatively charged hydroxyl group (OH^-) on adsorbed surfaces, allowing dichromate ions to diffuse more easily. Due to OH^- ions hindering dichromate ion diffusion at higher pH values, adsorption may decrease [58,59].

Alteration in the adsorbent dosage also affect the adsorption efficiency, during study it ranges from 0.1 to 0.5 g under room temperature, initial metal ion concentration (100 ppm), pH 4 and time duration of 90 min. Figure 7B depicted the change in removal rate as the dosage of adsorbent changes. The graph makes it very evident that when adsorbent dosage is increased, the percent removal of metal ions also increased. The large availability of functionalized empty sites on the adsorbent surface was the cause of this increase in removal efficiency. This upsurge in removal rate is due to an increase in the availability of functional groups and adsorption sites for metal ions. The adsorption process reaches equilibrium after a constant increase in the percentage of metal ions removed from the wastewater solution, which is caused by the overcrowding of adsorbent particles due to the overlapping of adsorption sites. The removal percentage of Cr (VI) ions were 76% [60,61].

3.2.2 Contact time and initial metal ion concentrations effect

During adsorption, contact time play vital role during batch adsorption experiments. In this study the adsorption rate was observed in the time ranges from 30 to 120 min, the nanocomposite adsorbent efficiency was determined. For this study, metal ion initial concentration ranges from 20 to 100 mg/L were evaluated, about 0.1 g adsorbent was added to the metal ion solution under constant pH 4 at room temperature. At every 30 min samples were taken out and analyse under UV spectrophotometer. Figure 7C Shows the upsurged removal percentages as the contact time increases and finally reaches equilibrium at 90 min. The observed results showed that the removal rate of chromium ions upsurge from 92 to 76%.

The impacts of initial metal ion concentration were analysed for 20, 40, 60, 80, and 100 ppm by optimizing other parameters such as pH (4), adsorbent dosage (0.1g), equilibrium contact time (90 min), at normal room temperature. Results described that on increasing the initial metal ion concentration from 20-100 ppm, the elimination percentage decreased from 92-76%. Figure 7D portrayed that on increasing the initial metal ions

concentrations, the removal percentage decreases simultaneously. This is happened due to low availability of active site onto the nanocomposite surface (Table 1). [62-64]

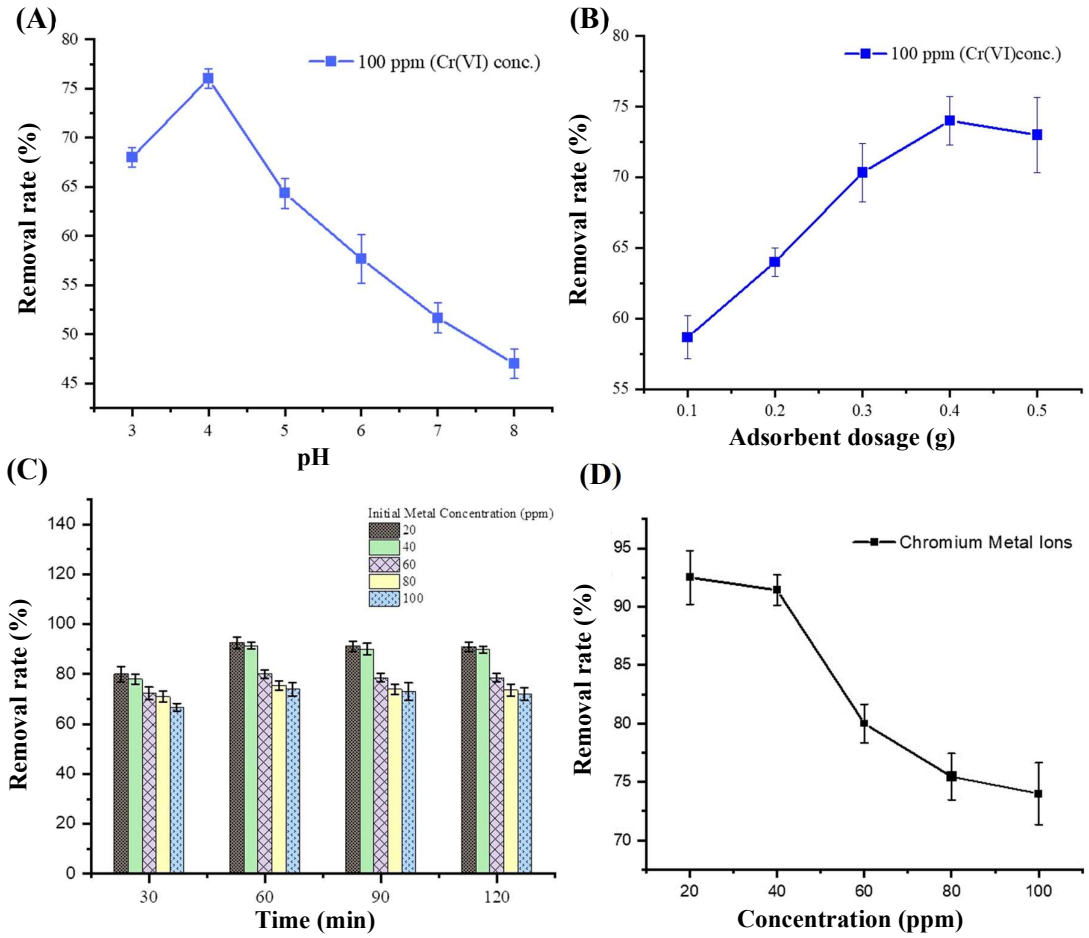

Figure 7 Graph representing effects of (A) pH (B) adsorbent dosage (C) Contact time (D) Initial metal ion on the removal of Cr (VI) ions onto nanocomposite.
**Experimental conditions: pH effect: pH range 3-9, Dosage 0.1, Contact time: 90 min; Dosage effect: Dose taken in range 0.1-0.5 g, contact time: 90 min, pH:4, Initial metal ion concentration: 100 mg/L; Contact time: Time ranges 30-120 min, initial metal ion conc. range 20-100 mg/L, pH:4, dosage-0.1 g; Initial metal ion effect: Range taken 20-100, pH:4, dosage-0.1 g, contact time 90 min.

Table 1 Showing adsorbed metal ion and removal rate of metal ions.

Initial metal ion concentration (ppm)	Adsorbed metal ions (mg/g)	Removal rate (%)
20	18.4	92.0
40	37.0	92.5
60	48.0	80.0
80	60.0	75.0
100	76.0	76.0

3.2.3 Langmuir and freundlich isotherms analysis (linear and nonlinear)

To understand how the adsorbent behaves when it comes to removing heavy metal ions through adsorption. A surface functional group's atom contributes electrons to the sorbate during the process of adsorption, by the donor-acceptor complexation mechanism. For the interaction between adsorbent and adsorbate (chromium metal ion) during the removal process, isotherm models viz., Langmuir and Freundlich (Linear and Non-linear) were examined in this study.

Monolayer homogenous adsorption is shown by Langmuir isotherm. Adsorbate ion multilayer heterogeneous adsorption is predicted by the Freundlich isotherm model. Langmuir and Freundlich isotherm fitting of experimental data Figure 6 depicts linear and nonlinear models, while Table 2 lists their computed parameters.

The correlation coefficient determines how well the isotherm model explains the adsorption process. The linearization curves of the Freundlich's and Langmuir isotherms shown in Figure 8 and the R^2 values in Table 2 demonstrate that the adsorption of Cr (VI) onto the surface of nanocomposite follows the Langmuir isotherm model. The outcomes showed that monolayer adsorption was responsible for the uptake of Cr (VI) ions on the nanocomposite surface. Additionally, the nanocomposite's maximum adsorption capacity (q_m) is 82.7 mg/g. The separation factor (R_L) was found 0.05, shows favourability for the adsorption of metal ions onto nanocomposite under optimized condition used in this study. [63]

Table 2 Isotherms parameters for adsorption of metal ion.

Adsorption Isotherms	Parameters	Values
Langmuir Isotherm (Linear form)	q_{max} (mg/g)	82.7
	K_L (L/mg)	0.191
	R_L	0.050
	R^2	0.92
Langmuir Isotherms (Non-linear form)	q_{max} (mg/g)	21.03
	K_L (L/mg)	3.79
	X^2	77.0
	R^2	0.88
Freundlich Isotherms (Linear form)	K_f	17.80
	1/n	0.432
	R^2	0.87
Freundlich Isotherms (Non-linear form)	K_f	18.49
	1/n	0.41
	X^2	51.61
	R^2	0.91

When predicting adsorption by using non-linear models, the solute absorptivity value (K_L=3.79 L/mg) were found higher than linear Langmuir model, comparatively the maximum adsorption capacity (q_m=21.03 mg/g) found to be much lesser, while in the Freundlich model, values of K_f and 1/n showing similarity in both the cases (linear and non-linear). On the basis of non-linear regression coefficient (R^2) the adsorption indicates good fit with Freundlich model (R^2=0.91) showing heterogenous behaviour of adsorption. Even so, the Chi-square test ($\chi 2$) indicated higher values in both the non-linear models. Therefore, as per linear models Langmuir isotherm showing good fit whereas in non-linear models Freundlich isotherm model shows best fit for the metal ion adsorption [65,66].

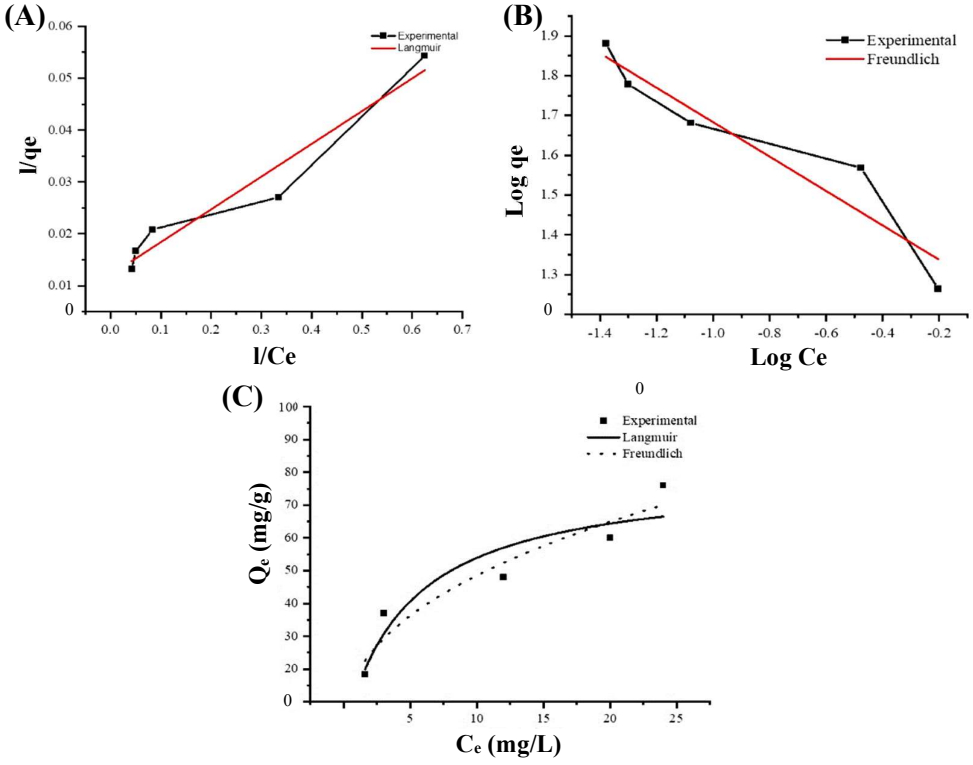

Figure 8 (A-B) Linear Langmuir & Freundlich Isotherm (C) Nonlinear Langmuir & Freundlich isotherms.

3.2.4 Adsorption kinetics (linear and nonlinear)

The kinetic study can be used to clarify how Cr (VI) absorption by nanocomposite is regulated. To explain how Cr (VI) ions adsorb on the surface of nanocomposite, linear and non-linear, pseudo 1st order and pseudo 2nd order kinetic models were utilized to match the experimental findings.

The parameters derived for the linear & nonlinear pseudo 1st order and pseudo 2nd order kinetic models that were used to fit the experimental data in Figure 9 and listed in Table 3. Compared to the pseudo 1st order model, the computed value from the linear pseudo-second-order model was closer to the experimental value of q_e. The rate constant K_1 value observed in the case of linear pseudo-first order is (-ve), indicating that the model is unfavourable for adsorption.

According to the $R^2 = 0.99$ values, the removal of Cr (VI) ions from the surface of nanocomposite also matches the pseudo-second-order model better than the pseudo-first-order model. Whereas, in case of non-linear kinetic models Pseudo first order show good fit according to $R^2 = 0.64$ value. The Chi-square test ($\chi 2$) showed higher values in both the non-linear models [67,68,69].

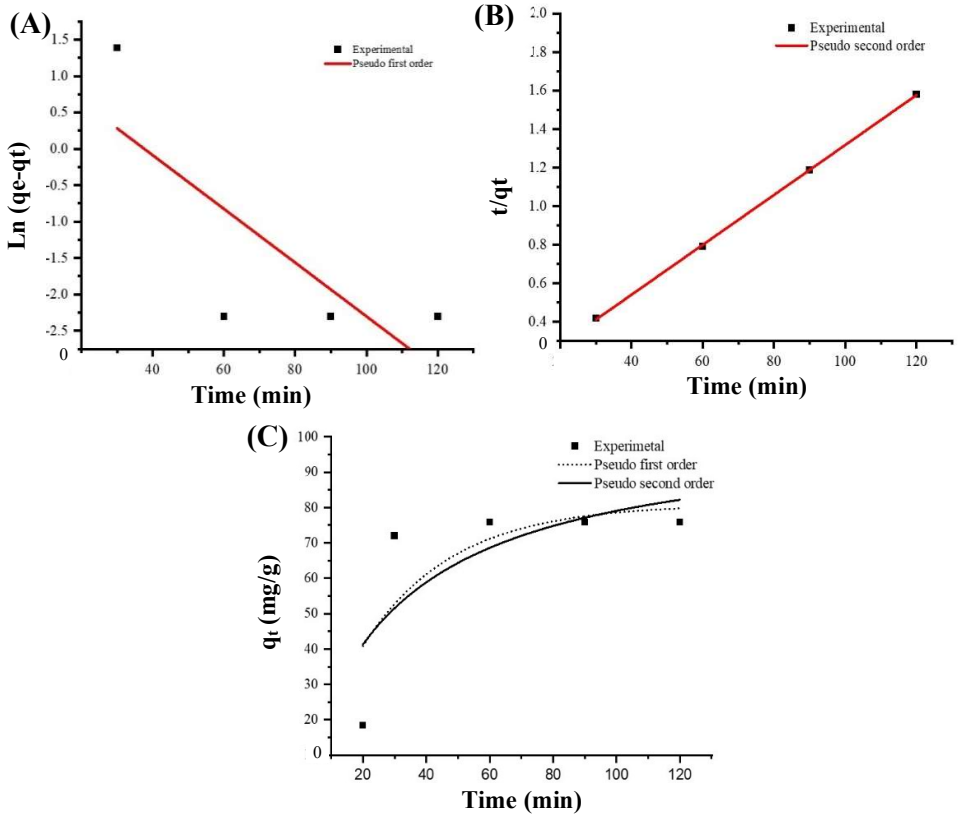

Figure 9 (A-B) Linear Pseudo 1st and Pseudo 2nd order (C) Nonlinear Pseudo 1st and Pseudo 2nd order.

Table 3 Kinetics parameters for adsorption of metal ion.

Order of Reaction	Parameters	Values
Pseudo 1st order (Linear form)	$q_{e\ Experimental}$ (mg/g)	76.0
	$q_{e\ calculated}$ (mg/g)	4.0
	K_1 (min)	-0.0003
	R^2	0.66
Pseudo 1st order (Non-linear form)	$q_{e\ calculated}$ (mg/g)	80.95
	K_1 (min)	0.035
	X^2	305.0
	R^2	0.64
Pseudo 2nd order (Linear form)	$q_{e\ calculated}$ (mg/g)	77
	K_2 (g mg/min)	0.01
	R^2	0.99
Pseudo 2nd order (Non-linear form)	$q_{e\ calculated}$ (mg/g)	102.51
	K_2 (min)	3.28
	X^2	345.0
	R^2	0.52

3.2.5 Thermodynamics parameters analysis

Temperature effect on the adsorption of chromium ions onto nanocomposite was investigated at 293, 298, 303, and 308 K at a fixed metal concentration (100 mg/L) and a constant pH of 4.0 over the course of 24 h. The evaluated parameters are shown in Table 4 and Figure 10A. The metal ion adsorption is spontaneous, favourable, and temperature-dependent, which is explained by the negative ΔG° values for all temperatures. Metal ions on the nanocomposite displayed endothermic behaviour according to positive values of ΔH°. The S° (+ve) results indicated that during adsorption, the degrees of freedom is increased at the solid-liquid interface. Metal ions replaced the coordinated water molecules during the adsorption process, increasing the unpredictability in the adsorbent-contaminant system. [70]

Table 4 Thermodynamics parameters for Cr (VI) removal onto nanocomposite.

Parameters		ΔG° (kJ/mol)				ΔH° (kJ/mol)	ΔS° J/ (mol K)
Pollutant	Adsorbent	293 K	298 K	303 K	308 K		
Cr^{+6}	nanocomposite	-2.83	-3.17	-3.49	-3.67	13.85	57.03

3.3 Regeneration/desorption

The reusability of the ChNC+MBA was detected by effective desorption rate shown in Figure 10 B. It became clear that metal ion regeneration with NaOH was less rapid than with HCl. Because the pH of the HCl solution is low, which facilitates the desorption process, the complexation of the chloride ion with the metal ion occurs easily. It was discovered that equilibrium was reached, and the maximum amount of adsorbed metal ions desorbed from the nanocomposite at a time span of 90 min. The effective desorption rate of the nanocomposite confirms it regeneration potential and likely to be repetitively used for metal ion adsorption study. In this study total five repetitive cycle was carried out which showed that after fourth cycle the removal efficiency of the nanocomposite get reduced.

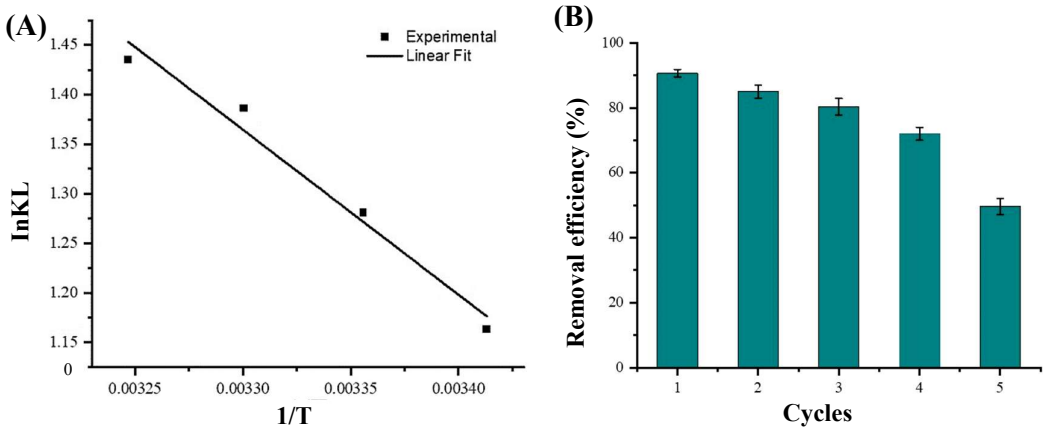

Figure 10 Graph of (A) thermodynamics adsorption and (B) nanocomposite adsorbent.

3.4 Advantage and disadvantages of synthesized nanocomposite

Biodegradable polymers like chitosan and nanocellulose were employed only in the formulation of the nanocomposite in this study, in contrast to previous works that had relied on a variety of synthetic polymers to increase the nanocomposite's efficacy, discuss in the introduction section. To combat fouling, a common issue with natural nanocomposites, we regenerate the material in a variety of reagent solutions, achieving a 90% removal rate after 4 regeneration cycles. The nanocomposite surface is protected against microbial growth by being kept in an airtight container between uses. One benefit of the produced nanocomposite is that the crosslinker MBA was utilized in a very little quantity (0.04 g) without a catalyst and reaction initiator. The washing step that comes after the hydrolysis process results in the production of acid water, which is one of the drawbacks. More chitosan and cellulose content added during nanocomposite fabrication makes it brittle. Results in weak bonding and becomes fragile. The synthesized nanocomposite is vulnerable to microbial attack if it is not stored in an airtight jar and not properly regenerated. The adsorption capacity of Cr (VI) onto ChNC+MBA nanocomposite was compared with the adsorption capacity of various other low-cost adsorbents, and the results are reported in Table 5.

Table 5 Various nanocomposite adsorbent for Cr (VI) removal.

Serial No.	Adsorbent	Q_{max} (mg/g)	pH	References
1	Common fig	29	3.5	[71]
2	Pine needle	21.50	2	[72]
3	Rice Straw	3.15	2	[73]
4	Eucalyptus bark	45	2	[74]
6	Almond shell	3.40	3	[75]
7	Treated waste newspaper	60	3	[76]
8	ChNC+MBA	76	4	Present study

4. Conclusion

ChNC+MBA membrane-based adsorbent was fabricated via blending and cross-linking to eliminate out the Cr (VI) from synthetic wastewater. The successful crosslinking of polymers was confirmed by FTIR by showing new functional group appearance due to formation of new bonds. The nanosuspension shown that all the particles are under nano-range after successful hydrolysis. The change in morphological structure was confirmed from SEM analysis. To know about efficacy of the ChNC+MBA to remove Cr (VI) ion, batch study was conducted. During study various other factors were optimized such as pH 4, optimum contact time 60 min for maximum removal and adsorbent dosage 0.1 g. For the suitability of the adsorption process, data were analysed using linear and nonlinear isotherm viz., Langmuir and Freundlich; Langmuir isotherm showing best fitted corelation with the experimental data in case of linear model whereas in case of nonlinear Freundlich showing the best fitted one. The evaluation of the linear and non-linear kinetic models also revealed that PSO (pseudo 2^{nd} order) and PFO (pseudo 1^{st} order) provided the best fits for the linear and non-linear cases, respectively. The adsorption mechanism is endothermic and spontaneous, according to thermodynamics research that was also conducted at various temperatures. Results showed that 0.1 M HCl satisfactorily regenerate the metal ions from the adsorbent, but it was noticed that after fourth cycle the efficiency get dropped. The utilized nanocomposite was desorbed to minimize fouling problem. To determine the nanocomposite's capacity for removal, an ionic effect research was applied to it. The ChNC+MBA membrane-based adsorbent was subsequently discovered to be efficient in terms of cost and suitable for the successful removal of heavy metal ions from wastewater.

5. Acknowledgements

The Nanomaterial Lab at Graphic Era (deemed to be) University in Dehradun, which is supported by the Technology Mission Division of the Department of Science and Technology of India, is acknowledged by the authors for offering research facilities and supervision.

6. References

[1] Milewski A, Lezzaik K, Rotz R. Sensitivity analysis of the groundwater risk index in the Middle East and North Africa region. Environ Process. 2020;7:53-71.

[2] Ajiboye TO, Oyewo OA, Onwudiwe DC. Simultaneous removal of organics and heavy metals from industrial wastewater: a review. Chemosphere. 2021;262:128379.

[3] Awual MR, Hasan MM, Iqbal J, Islam A, Islam MA, Asiri AM, et al. Naked-eye lead (II) capturing from contaminated water using innovative large-pore facial composite materials. Microchem J. 2020;154:104585.

[4] Awual MR. New type mesoporous conjugate material for selective optical copper (II) ions monitoring & removal from polluted waters. Chem Eng J. 2017;307:85-94.

[5] Zhu F, Zheng YM, Zhang BG, Dai YR. A critical review on the electrospun nanofibrous membranes for the adsorption of heavy metals in water treatment. J Hazard Mater. 2021;401:123608.

[6] Wan Z, Li M, Zhang Q, Fan Z, Verpoort F. Concurrent reduction-adsorption of chromium using m-phenylenediamine-modified magnetic chitosan: kinetics, isotherm, and mechanism. Environ Sci Pollut Res. 2018;25:17830-17841.

[7] Awual MR. An efficient composite material for selective lead (II) monitoring and removal from wastewater. J Environ Chem Eng. 2019;7(3):103087.

[8] Ravikumar KV, Kumar D, Rajeshwari A, Madhu GM, Mrudula P, Chandrasekaran N, et al. A comparative study with biologically and chemically synthesized nZVI: applications in Cr (VI) removal and ecotoxicity assessment using indigenous microorganisms from chromium-contaminated site. Environ Sci Pollu Res. 2016;23:2613-2627.

[9] Awual MR, Hasan MM, Znad H. Organic-inorganic based nano-conjugate adsorbent for selective palladium (II) detection, separation and recovery. Chem Eng J. 2015;259:611-619.
[10] Ogata F, Nagai N, Itami R, Nakamura T, Kawasaki N. Potential of virgin and calcined wheat bran biomass for the removal of chromium (VI) ion from a synthetic aqueous solution. J Environ Chem Eng. 2020; 8:103710.
[11] Tiadi N, Mohanty M, Mohanty CR, Panda HP. Studies on adsorption behavior of an industrial waste for removal of chromium from aqueous solution. S Afr J Chem Eng. 2017;23:132-138.
[12] Vakili M, Deng S, Li T, Wang W, Wang W, Yu G. Novel crosslinked chitosan for enhanced adsorption of hexavalent chromium in acidic solution. Chem Eng Sci. 2018;347:782-790.
[13] United States Environmental Protection Agency (USEPA). Basic information about chromium in drinking water, http://water.epa.gov/drink/contaminants/basicinformation/chromium.cfm [accessed 11 December 2022].
[14] Yao W, Rao P, Lo IM, Zhang W, Zheng W. Preparation of cross-linked magnetic chitosan with quaternary ammonium and its application for Cr (VI) and P (V) removal. J Environ Sci. 2014;26(12):2379-2386.
[15] Awual MR. A novel facial composite adsorbent for enhanced copper (II) detection and removal from wastewater. Chem Eng J. 2015;266:368-375.
[16] Yang Z, Chai Y, Zeng L, Gao Z, Zhang J, Ji H. Efficient removal of copper ion from wastewater using a stable chitosan gel material. Molecules. 2019;24:4205.
[17] Li H, Gao P, Cui J, Zhang F, Wang F, Cheng J. Preparation and Cr (VI) removal performance of corncob activated carbon. Environ Sci Pollut Res. 2018;25:20743-20755.
[18] Hasan MN, Shenashen MA, Hasan MM, Znad H, Awual MR. Assessing of cesium removal from wastewater using functionalized wood cellulosic adsorbent. Chemosphere. 2021;270:128668.
[19] Nandal M, Hooda R, Dhania G. Tea wastes as a sorbent for removal of heavy metals from wastewater. Int J Curr Eng Technol. 2014;4:244-247.
[20] Dhevagi P, Priyatharshini S, Ramya A. Response surface methodology as a tool for optimization of metal adsorption by banana peel biochar. Int J Curr Microbiol Appl Sci. 2019;8:996-1009.
[21] Enniya I, Rghioui L, Jourani A. Adsorption of hexavalent chromium in aqueous solution on activated carbon prepared from apple peels. Sustain Chem Pharm. 2018;7:9-16.
[22] Atenas MG, Schroeder SL. Sustainable natural adsorbents for heavy metal removal from wastewater: lead sorption on pine bark (*Pinus radiata* D. Don). Surf Interface Anal. 2015;47:996-1000.
[23] Sugashini S, Begum KM. Preparation of activated carbon from carbonized rice husk by ozone activation for Cr (VI) removal. New Carbon Mater. 2015;30:252-261.
[24] Kabir MM, Akter MM, Khandaker S, Gilroyed BH, Alam DM, Hakim M, et al. Highly effective agro-waste based functional green adsorbents for toxic chromium (VI) ion removal from wastewater. J Mol Liq. 2022;347:118327.
[25] Awual MR, Hasan MM, Khaleque MA, Sheikh MC. Treatment of copper (II) containing wastewater by a newly developed ligand based facial conjugate materials. Chem. Eng. J. 2016;288:368-376.
[26] Son EB, Poo KM, Mohamed HO, Choi YJ, Cho WC, Chae KJ. A novel approach to developing a reusable marine macro-algae adsorbent with chitosan and ferric oxide for simultaneous efficient heavy metal removal and easy magnetic separation. Bioresour Technol. 2018;259:381-387
[27] Awual MR, Alharthi NH, Hasan MM, Karim MR, Islam A, Znad H, et al. Inorganic-organic based novel nano-conjugate material for effective cobalt (II) ions capturing from wastewater. Chem Eng J. 2017;324:130-139.
[28] Nemr EA, Ismail MNM, Ashry ESH, Hamid HA, Novel simple modification of chitosan as adsorptive agent for removal of Cr6+ from aqueous solution. Egypt J Chem. 2020;63(4):21-22.
[29] Gierszewska M, Jakubowska E, Kruszkowska OE. Effect of chemical crosslinking on properties of chitosan-montmorillonite composites. Polym Test. 2019;77:105872.
[30] Pan C, Qian J, Zhao C, Yang H, Zhao X, Guo H. Study on the relationship between crosslinking degree and properties of TPP crosslinked chitosan nanoparticles. Carbohydr Polym. 2020;241:116349.
[31] Tahira I, Aslam Z, Abbas A, Mehboob M, Ali S, Asghar A. Adsorptive removal of acidic dye onto grafted chitosan: a plausible grafting and adsorption mechanism. Int J Biol Macromol. 2019;136:1209-1218.
[32] Bidgoli H, Zamani A, Taherzadeh MJ. Effect of carboxymethylation conditions on the water-binding capacity of chitosan-based superabsorbents. Carbohydr Res. 2010;345:2683-2689.
[33] Sofla KMS, Mortazavi S, Seyfi J. Preparation and characterization of polyvinyl alcohol/chitosan blends plasticized and compatibilized by glycerol/polyethylene glycol. Carbohydr Poly. 2020;232:115784.
[34] Awual MR. Innovative composite material for efficient and highly selective Pb (II) ion capturing from wastewater. J Mol Liq. 2019;284:502-510.
[35] Wei J, Yang Z, Sun Y, Wang C, Fan J, Kang G, et al. Nanocellulose-based magnetic hybrid aerogel for adsorption of heavy metal ions from water. J Mater Sci. 2019;54(8):6709-6718.

[36] Awual MR, Hasan MM, Islam A, Asiri AM, Rahman MM. Optimization of an innovative composited material for effective monitoring and removal of cobalt (II) from wastewater. J Mol Liq. 2020;298:112035.
[37] Tshikovhi A, Mishra SB, Mishra AK. Nanocellulose-based composites for the removal of contaminants from wastewater. Int J Biol Macromol. 2020;152:616-632.
[38] Norrrahim FMN, Kasim MNA, Knight VF, Misenan MS, Janudin N, Shah ANA, et al. Nanocellulose: a bioadsorbent for chemical contaminant remediation. RSC Adv. 2021;11(13):7347-7368.
[39] Kabiri K, Mirzadeh H, Mehr ZMJ. Undesirable effects of heating on hydrogels. J Appl Polym Sci. 2008;110(6):3420-3430.
[40] Pourjavadi A, Mahdavinia GR. Superabsorbency, pH-sensitivity and swelling kinetics of partially hydrolyzed chitosan-g-poly (acrylamide) hydrogels. Turk J Chem. 2006;30(5):595-608.
[41] Ranjha NM, Ayub G, Naseem S, Ansari MT. Preparation and characterization of hybrid pH-sensitive hydrogels of chitosan-co-acrylic acid for controlled release of verapamil. J Mater Sci Mater Med. 2010;21(10):2805-2816.
[42] Brugnerotto J, Lizardi J, Goycoolea FM, Monal AW, Desbrières J, Rinaudo M. An infrared investigation in relation with chitin and chitosan characterization. Polymer. 2001;42:3569-3580.
[43] Lagaron JM, Saiz FP, Ocio MJ. Using ATR-FTIR spectroscopy to design active antimicrobial food packaging structures based on high molecular weight chitosan polysaccharide. J Agri Food Chem. 2007;55(7):2554-2562.
[44] Ziani K, Oses J, Coma V, Maté JI. Effect of the presence of glycerol and Tween 20 on the chemical and physical properties of films based on chitosan with different degree of deacetylation. LWT Food Sci Technol. 2008;41(10):2159-2165.
[45] He G, Xiang C, Yin Y, Cai W, Ke W, Kong Y, et al. Preparation and antibacterial properties of O-carboxymethyl chitosan/lincomycin hydrogels. J Biomater Sci Polym Ed. 2015;27:370-384.
[46] Khandaker S, Chowdhury MF, Awual MR, Islam A, Kuba T. Efficient cesium encapsulation from contaminated water by cellulosic biomass based activated wood charcoal. Chemosphere. 2021;262:127801.
[47] Avşar A, Gökbulut Y, Ay B, Serin S. A novel catalyst system for the synthesis of N, N′-Methylenebisacrylamide from acrylamide. Designed monomers and polymers. 2017;20(1):434-440.
[48] Mandal A, Chakrabarty D. Isolation of nanocellulose from waste sugarcane bagasse (SCB) and its characterization. Carbo Poly. 2011;86(3):1291-1299.
[49] Li J, Wei X, Wang Q, Chen J, Chang G, Kong L, et al. Homogeneous isolation of nanocellulose from sugarcane bagasse by high pressure homogenization. Carbo Poly. 2012;90(4):1609-1613.
[50] Travlou NA, Kyzas GZ, Lazaridis NK, Deliyanni EA. Functionalization of graphite oxide with magnetic chitosan for the preparation of a nanocomposite dye adsorbent. Langmuir. 2013,29:1657-1668.
[51] Colom X, Carrillo F, Nogués F, Garriga P. Structural analysis of photodegraded wood by means of FTIR spectroscopy. Poly Degrad Stab. 2003;80(3):543-549.
[52] Kabir A, Dunlop MJ, Acharya B, Bissessur R, Ahmed M. Water recycling efficacies of extremely hygroscopic, antifouling hydrogels. RSC Adv. 2018;8(66):38100-38107.
[53] Samuel MS, Bhattacharya J, Raj S, Santhanam N, Singh H, Singh NP. Efficient removal of Chromium (VI) from aqueous solution using chitosan grafted graphene oxide (CS-GO) nanocomposite. Intern J Bio Macromole. 2019;121:285-292.
[54] Zhang H, Shen H, Lan J, Wu H, Wang L, Zhou J. Dual-network polyacrylamide/carboxymethyl chitosan-grafted-polyaniline conductive hydrogels for wearable strain sensors. Carbo Poly. 2022;295:119848.
[55] Ismael MN, Nemr A, Ashry ES, Hamid AH. Removal of hexavalent chromium by cross-linking chitosan and N, N'-methylene bis-acrylamide. Environ Proc. 2020;7(3):911-930.
[56] Islam A, Teo SH, Awual MR, Yap TYH. Assessment of clean H2 energy production from water using novel silicon photocatalyst. J Clean Prod. 2020;244:118805.
[57] Bai RS, Abraham TE. Studies on chromium (VI) adsorption-desorption using immobilized fungal biomass. Bioreso Technol. 2003;87(1):17-26.
[58] Awual MR. A facile composite material for enhanced cadmium (II) ion capturing from wastewater. J Environ Chem Eng. 2019;7:103378.
[59] Ba S, Alagui A, Hajjaji M. Retention and release of hexavalent and trivalent chromium by chitosan, olive stone activated carbon, and their blend. Environ Sci Pollut Res. 2018,25:19585-19604.
[60] Ali ME. Synthesis and adsorption properties of chitosan-CDTA-GO nanocomposite for removal of hexavalent chromium from aqueous solutions. Arab J Chem. 2018;11(7):1107-1116.
[61] Awual MR, Yaita T, Kobayashi T, Shiwaku H, Suzuki S. Improving cesium removal to clean-up the contaminated water using modified conjugate material. J Environ Chem Eng. 2020;8:103684.
[62] Sun X, Li Q, Yang L, Liu H. Chemically modified magnetic chitosan microspheres for Cr (VI) removal from acidic aqueous solution. Particuology. 2016;26:79-86.

[63] Dehghani MH, Sanaei D, Ali I, Bhatnagar A. Removal of chromium (VI) from aqueous solution using treated waste newspaper as a low-cost adsorbent: kinetic modeling and isotherm studies. J Mol Liq. 2016;215:671-679.
[64] Vilela PB, Dalalibera A, Duminelli EC, Becegato VA, Paulino AT. Adsorption and removal of chromium (VI) contained in aqueous solutions using a chitosan-based hydrogel. Environ Sci Poll Res. 2019;26(28):28481-28489.
[65] Kubra KT, Salman MS, Hasan MN, Islam A, Teo SH, Hasan MM, et al. Sustainable detection and capturing of cerium (III) using ligand embedded solid-state conjugate adsorbent. J Mol Liq. 2021;338:116667.
[66] Foo KY, Hameed BH. Insights into the modeling of adsorption isotherm systems. Chem Eng J. 2010;156:2-10.
[67] Dey A, Singh R, Purkait MK. Cobalt ferrite nanoparticles aggregated schwertmannite: a novel adsorbent for the efficient removal of arsenic. J Water Process Eng. 2014;3:1-9.
[68] Tu YJ, You CF, Chang CK, Wang SL, Chan TS. Arsenate adsorption from water using a novel fabricated copper ferrite. Chem Eng J. 2012;198-199:440-448.
[69] Naushad M, Alqadami AA, Kahtani AA, Ahamad T, Awual MR, Tatarchuk T. Adsorption of textile dye using para-aminobenzoic acid modified activated carbon: Kinetic and equilibrium studies. J Mol Liq. 2019;296:112075.
[70] Bhattacharya AK, Naiya TK, Mandal SN, Das SK. Adsorption, kinetics and equilibrium studies on removal of Cr (VI) from aqueous solutions using different low-cost adsorbents. Chem. Eng J. 2008;137(3):529-541
[71] Gupta VK, Pathania D, Sharma S, Agarwal S, Singh P. Remediation of noxious chromium (VI) utilizing acrylic acid grafted lignocellulosic adsorbent. J Mol Liq. 2013;177:343-52.
[72] Dakiky M, Khamis M, Manassra A, Mer'Eb M. Selective adsorption of chromium (VI) in industrial wastewater using low-cost abundantly available adsorbents. Adv Environ Res. 2002;6(4):533-540.
[73] Gao H, Liu Y, Zeng G, Xu W, Li T, Xia W. Characterization of Cr (VI) removal from aqueous solutions by a surplus agricultural waste-rice straw. J Hazard Mater. 2008;150(2):446-452.
[74] Sarin V, Pant K. Removal of chromium from industrial waste by using eucalyptus bark. Bioresour Technol. 2006;97(1):15-20.
[75] Pehlivan E, Altun T. Biosorption of chromium (VI) ion from aqueous solutions using walnut, hazelnut and almond shell. J Hazard Mater. 2008;155(1-2):378-384.
[76] Dehghani MH, Sanaei D, Ali I, Bhatnagar A. Removal of chromium (VI) from aqueous solution using treated waste newspaper as a low-cost adsorbent: kinetic modeling and isotherm studies. J Mol Liq. 2016;215:671-679.